Electronic Supplementary Information

Anomalous Compression of a Weakly CH···O Bonded Nonlinear Optical Molecular Crystal

Weizhao Cai,[a] Jiangang He,[b] Wei Li*[c] and Andrzej Katrusiak*[a]

[a] *Faculty of Chemistry, Adam Mickiewicz University, Umultowska 89b, Poznań 61-614, Poland*

[b] *School of Applied and Engineering Physics, Cornell University, Ithaca, New York 14853, USA*

[c] *Department of Materials Science and Metallurgy, University of Cambridge, Cambridge CB3 0FS, UK*

Experiment Details

High-pressure X-ray experiment

3-Methyl-4-nitropyridine *N*-oxide, $C_6H_6N_2O_3$, POM, was re-crystallized from saturated acetone solution by evaporating the solvent. One single crystal of dimensions 0.37×0.28×0.15 mm was selected and glued in a glass fiber with nail varnish, and the crystal data at ambient condition were collected on diffractometer Oxford Diffraction Xcalibur *Eos*, with graphite-monochromated MoKα radiation (λ = 0.71073 Å).

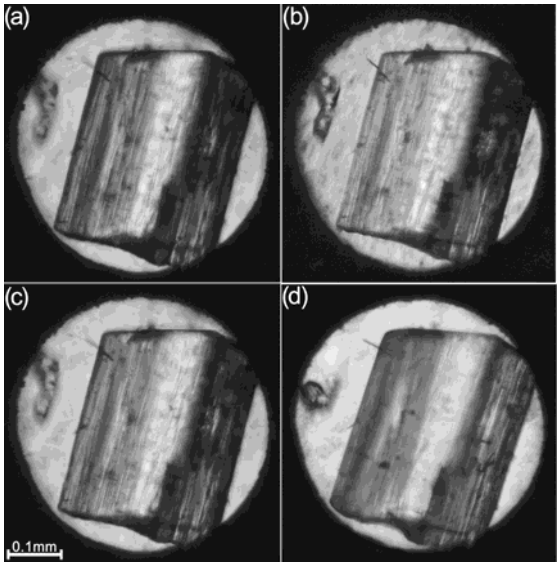

Fig. S1 Isothermal compression of the POM single crystal in the DAC chamber at: (a) 0.07 GPa, (b) 0.34 GPa; (c) 0.52 GPa; and (d) 0.81 GPa, all at 296 K. Two ruby chips for pressure calibration lie on the left top side of the chamber.

Then the same single crystal was mounted in a modified Merrill-Bassett diamond-anvil cell (DAC).[1] The gasket was made of 0.3 mm thick tungsten foil and the initial diameter of the spark-eroded hole was 0.5 mm. Since POM is soluble in most of traditional hydrostatic fluids, glycerol (its hydrostatic limit up to 4.0 GPa)[2] was finally chosen as the pressure transmitting medium. Pressure was calibrated with a Photon Control spectrometer by the ruby-fluorescence method with a precision of 0.04 GPa.[3] The first single crystal high-pressure diffraction data were collected at 0.07 GPa, other data were recorded with pressure increased gradually to 0.81 GPa/296 K. The single-crystal quality in the DAC chamber was controlled by using the microscope (see Fig. S1) and by

inspecting high-angle reflections.

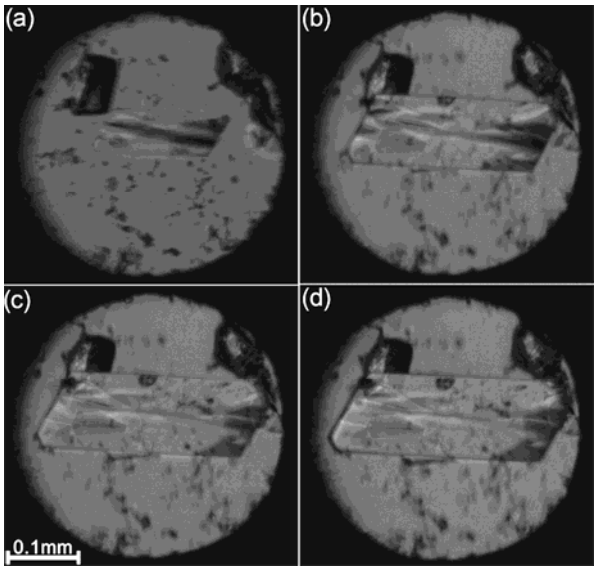

Fig. S2 *In situ* isochoric growth of the POM single crystal in methanol solution: (a) one seed at 423 K; (b) 403 K; (c) 358 K; and (d) at 1.29 GPa/296 K. Two ruby chips for pressure calibration lie at the top left and right sides of the chamber.

We attempted the *in situ* growth of POM single crystal in the DAC to check the crystal stability. A phase transition in POM was proposed.[4] We selected several small POM crystals and loaded them to the DAC chamber, then topped with methanol (hydrostatic limit: 3.6 GPa).[5] After pressure increasing to 1.29 GPa, the DAC was heated by a hot-air gun to 423 K when all crystals except one seed dissolved. Then temperature was slowly decreased to room temperature, to allow the single crystal to grow. Finally, a plate-like single crystal 0.32×0.18×0.10 mm in size was obtained and the pressure stabilized at 1.29 GPa/296 K (Fig. S2). Diffraction data were collected for this single crystal and then at 1.58, 2.04, 2.68, 3.57 GPa/296 K, respectively.

Single-crystal high-pressure diffraction data were collected on the same diffractometer as the data collected at ambient condition, with graphite-monochromated MoKα radiation (λ = 0.71073 Å). The centering of the DAC was performed by the gasket-shadowing method.[6] CrysAlisPro software was used for the data collection and the preliminary reduction of the data.[7] After the intensities were corrected for the effects of DAC absorption, sample shadowing by the gasket and the sample absorption, the diamond reflections were eliminated.[8] The ambient-pressure structure was applied as the

starting model for full-matrix least-squares refinements on high-pressure data. H-Atoms were located from the molecular geometry, with the C−H distances equal to 0.93 (pyridine ring) and 0.96 Å (methyl group), respectively. The anisotropic factors U_{ij} of some non-hydrogen C, N and O atoms were restrained to approximate isotropic values with instruction ISOR 0.01.

Variable-Temperature Single Crystal X-Ray Diffraction

Variable temperature data were collected with an Oxford Diffraction diffractometer Xcalibur *Eos* (MoKα radiation, λ = 0.71073 Å) for one single crystal 0.30×0.30×0.20 mm in size. The diffraction data were initially collected at 300 K and then a series of data sets were recorded at intervals of 15 K down to 120 K. Crystal data, refinement details for the variable-temperature and high-pressure structures are listed in Tables S1 and S2.

Nanoindentation Methodology of Single-Crystals

Nanoindentation experiments were performed at room temperature with the indenter aligned normal to the {100}, {010} or {001} facets using an MTS NanoIndenter® XP (MTS Corp., Eden Prairie, MN).[9] In the continuous stiffness measurement (CSM) mode, where indentation is controlled by displacement, the Young's modulus (E_s) was measured using a three-sided pyramidal Berkovich tip (radius ~100 nm). With a strain rate of 0.05 s^{-1}, the load (P) and the displacement (h) were monitored continuously during the experiment until a maximum displacement of 1000 nm was reached, at which point the indenter was held for 30 s before unloading at the same strain rate in order to minimize creep effects. The average contact pressure during loading was determined according to the literature.[10]

Optical Property Calculations

The optical property calculations were performed based on the experimental structures with relaxed C-H bond by using vdW-DF method of optB86b functionals,[11] as implemented in the VASP code.[12] The energy cutoff of the plane-wave basis functions was set to be 600 eV. The interactions between electron and ion were described by projector augmented wave (PAW) potential.[13] The valence electrons of the elements included H, $1s^1$; C, $2s^2p^2$; N, $2s^2p^3$ and O, $2s^2p^4$. Generalized gradient approximation

(GGA) in the scheme of Perdew-Burke-Eruzerhof (PBE) was used to describe the exchange and correlative potential of electron-electron interactions.[14] The *k* point of first Brillouin zone was sampled as the 2×6×8 Monkhorst-Pack scheme. Under the restriction of crystal symmetry and Kleinman's symmetry, there is only one independent element ($d_{14} = d_{25} = d_{36}$) in space group $P2_12_12_1$. Therefore only $\chi^{(2)}_{xyz}(-2\omega;\omega;\omega)$ was calculated ($\chi^{(2)}_{xyz}(-2\omega;\omega;\omega) = 2d_{36}$).[15]

In this paper, the second-order susceptibilities $\chi^{(2)}_{xyz}(-\omega_3;\omega_1,\omega_2)$ were calculated within anharmonic oscillator (AHO) model:[16]

$$2d_{xyz}(-\omega_3;\omega_1,\omega_2) = \chi^{(2)}_{xyz}(-\omega_3;\omega_1,\omega_2) = F\chi^{(1)}_{xx}(\omega_3)\chi^{(1)}_{yy}(\omega_1)\chi^{(1)}_{zz}(\omega_2)$$

where coefficient $F = m\omega_0^2/(N^2e^3d)$ can be calculated by mass (m) and charge (e) of electron, density number of unit cell (N), lattice constant (d), and response frequency (ω_0). The first-order susceptibly $\chi^{(1)}_{mm}(\omega_n)$ can be calculated from dielectric function $\varepsilon(\omega)$ by using $\chi^{(1)}(\omega)_{mm} = [\varepsilon(\omega)_{mm} - 1]/4\pi$. The dielectric function can be directly obtained from VASP calculations. Noteworthy, the response peak of frequency-dependent SHG coefficient is underestimated because of the well-known band gap underestimation of standard DFT method.

In order to explore the effect of molecular structure on the enhanced nonlinear optical property of POM under pressure, we further studied the linear and nonlinear optical properties of the POM molecule. The molecular structures of POM were relaxed and their dipole moments μ, first-order polarizabilities α, and second-order polarizabilities β based on the relaxed structure were calculated using the DFT method with B3LYP exchange-correlation functional and 6-311+G(d,p) basis set, as implemented in *Gaussian 03* package.[17] Molecular structures at 0.1 MPa, 0.07, 0.12, 0.34, 0.83, 1.29, 2.04, 2.68 and 3.57 GPa were fully relaxed, except the torsion angle τ(O2−N2−C3−C4) constrained to the values in crystal to simulate the effects of pressure.

The gas-phase calculations have revealed that the torsion angle τ in most energetically stable conformer is equal to 4.6º, which is different from planar conformer postulated earlier.[18] The τ twisting is due to steric effects. Our gas-phase calculations reveal the potential energy difference of POM molecule between 0.12 GPa (τ = 19.4(8)º) and 0.1 MPa (τ = 15.7(1)º) is 0.17 kJ mol^{-1}. Further hydrostatic compression only lowers the

potential energy to about 0.08 kJ mol^{-1} at 3.57 GPa (τ = 12.1º), relative to the molecular conformer at ambient pressure.

The magnitudes of dipole moment μ, mean polarizability <α>, and second-order polarizability β become larger as the torsion angle is reduced with increasing pressure. To understand these results, we performed excited state calculations. The components of α and β can be estimated by the low-energy dipole-allowed electronic transitions within two-state model,[19]

$$\alpha_{ii} \propto \frac{M_{ii}^{eg}}{\Delta E^{eg}}$$

$$\beta_{iii} \propto \frac{\Delta\mu_i^{eg}(M_{ii}^{eg})^2}{(\Delta E^{eg})^2}$$

where M_{ii}^{eg} and ΔE^{eg} are the transition dipole moment in i direction and transition energy from ground state (g) to excited state (e), respectively. $\Delta\mu_i^{eg} = \mu_i^e - \mu_i^g$ is the change of dipole moment from ground state to excited state in direction i. M_{ii}^{eg} and $\Delta\mu_i^{eg}$ were calculated by using time-dependent (TD) DFT method. Our calculations reveal that M_{xx}^{eg} and $\Delta\mu_x^{eg}$ are dominating, in line with polarizability and second-order polarizability calculations that α_{xx} and β_{xxx} are the largest components (Tables S7 and 8). As shown in Table S9, M_{xx}^{eg}, $\Delta\mu_x^{eg}$ and oscillator strength decrease with torsion angle increasing, while ΔE^{eg} increases. This feature agrees well with our polarizability and second-order polarizability calculations that both of them are decreasing when the torsion angle increases. Fig. S15 shows the front orbitals involved in the lowest dipole-allowed excitation of POM. The charge transfer along the x direction is clearly seen. The large torsion angle blocks the charge transfer along the x direction, so as to small values of M_{xx}^{eg} and $\Delta\mu_x^{eg}$.

The definition of mean dipole moment <μ>, mean polarizability <α> and the total second-order polarizability β_{tot} and tensor β_x are given as following:

$$\mu = (\mu_x^2 + \mu_y^2 + \mu_z^2)^{1/2}$$

$$\langle\alpha\rangle = \frac{1}{3}(\alpha_{xx} + \alpha_{yy} + \alpha_{zz})$$

$$\beta_{\text{total}} = (\beta_x^2 + \beta_y^2 + \beta_z^2)^{1/2} \quad \text{in which} \quad \beta_i = \beta_{iii} + \beta_{ijj} + \beta_{ikk} (i, j, k = x, y, z)$$

$$\beta_{\text{vec}} = \beta_{\text{x}} = \beta_{\text{xxx}} + \beta_{\text{xyy}} + \beta_{\text{xzz}}$$

The related calculated results are listed in Tables S7 and 8.

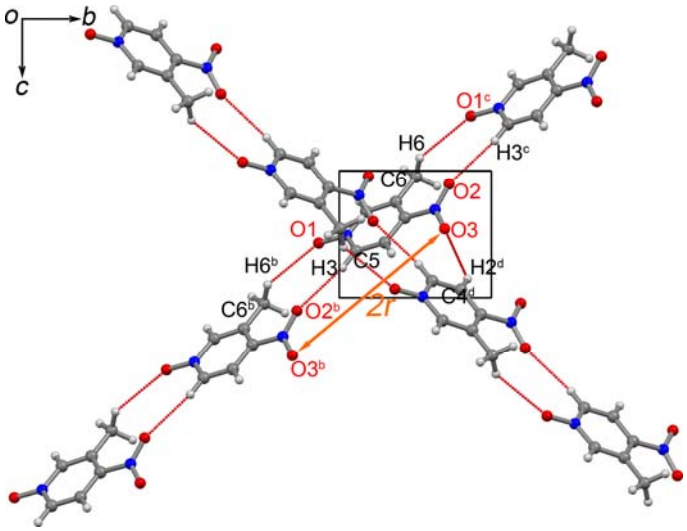

Fig. S3 The hinged structure of POM at 0.1 MPa viewed along [100] direction. Intermolecular contacts C−H···O (red dashes) have been indicated. For the clarity, only one pair of chains along diagonal directions [011] and $[0\bar{1}1]$ were displayed. The parameter *r* is half of the unit-cell *bc* diagonal (equal to half of the translation along $[0\bar{1}1]$ direction).

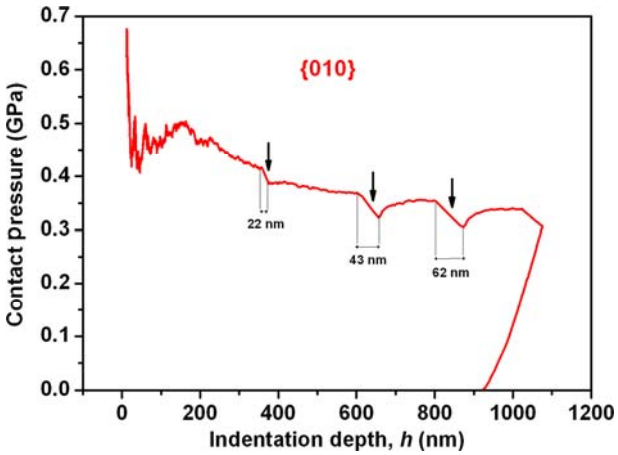

Fig. S4 The contact pressure as a function of penetration depth throughout the course of loading and unloading, measured with a Berkovich tipped indenter on {010} face. The 'pop-ins' are indicated as arrows, and their magnitudes are labelled accordingly.

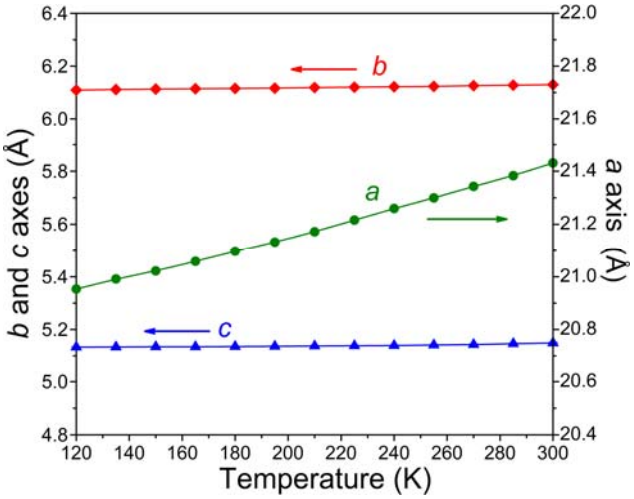

Fig. S5 The unit-cell dimensions of POM as a function of temperature between 120 and 300 K. For all the points, the error bars are smaller than the symbols.

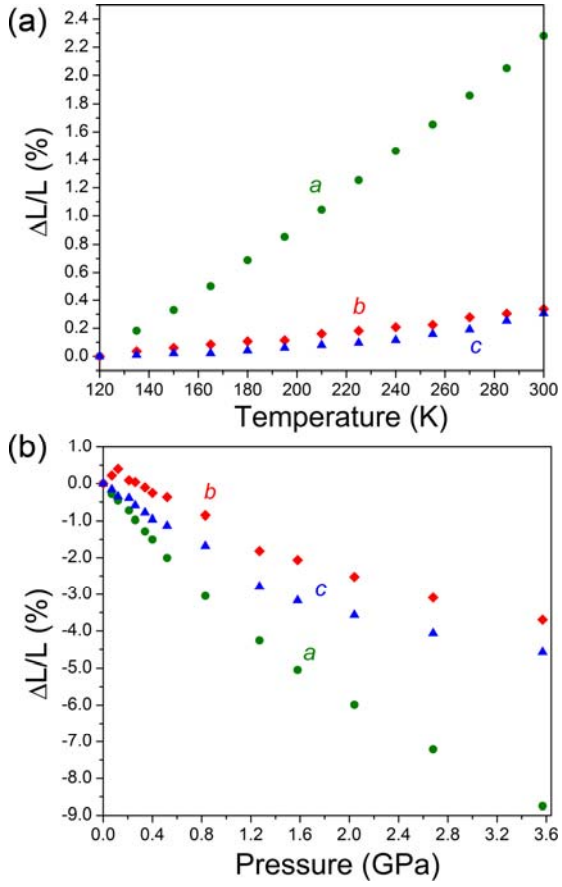

Fig. S6 Relative lattice-parameters variation of POM observed with changes in (a) temperature and (b) hydrostatic pressure. In the main plots error bars are smaller than the symbols used.

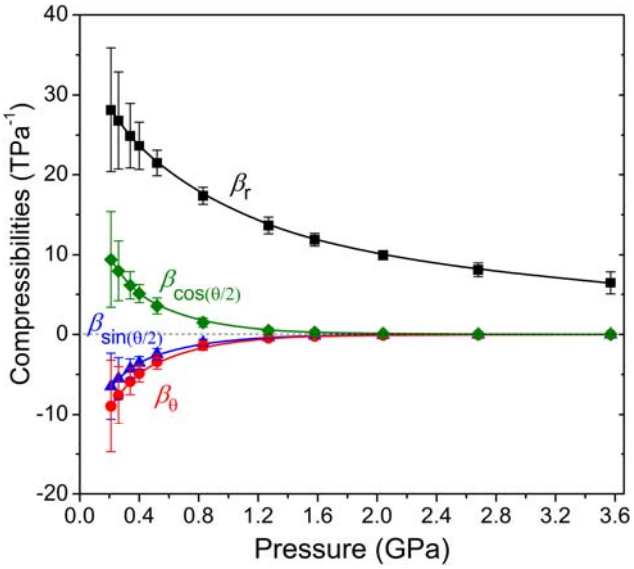

Fig. S7 Pressure dependence of compressibilities $\beta = -(\partial \ln w/\partial p)_T$ for parameter w equal to: r (black squares), hinge angle θ (red circles), $\sin(\theta/2)$ (blue triangles) and $\cos(\theta/2)$ (green diamonds) in phase II of POM in the range of 0.21 to 3.57 GPa calculated by *PASCal* (ref 20).

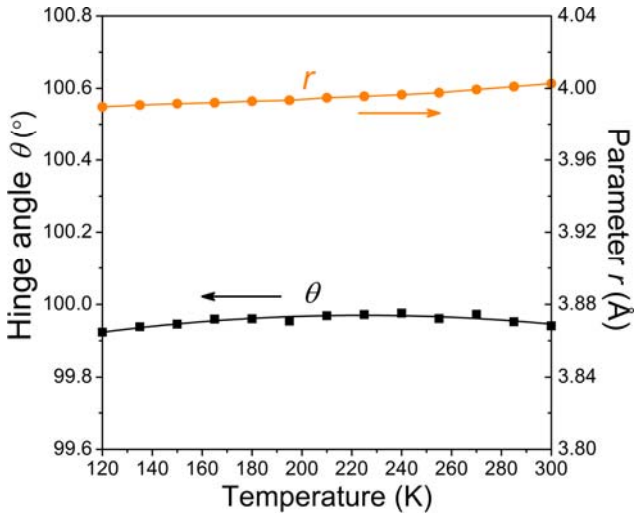

Fig. S8 The temperature dependence of hinge angle θ and parameter r from 120 to 300 K. For all the points, the error bars are smaller than the symbols.

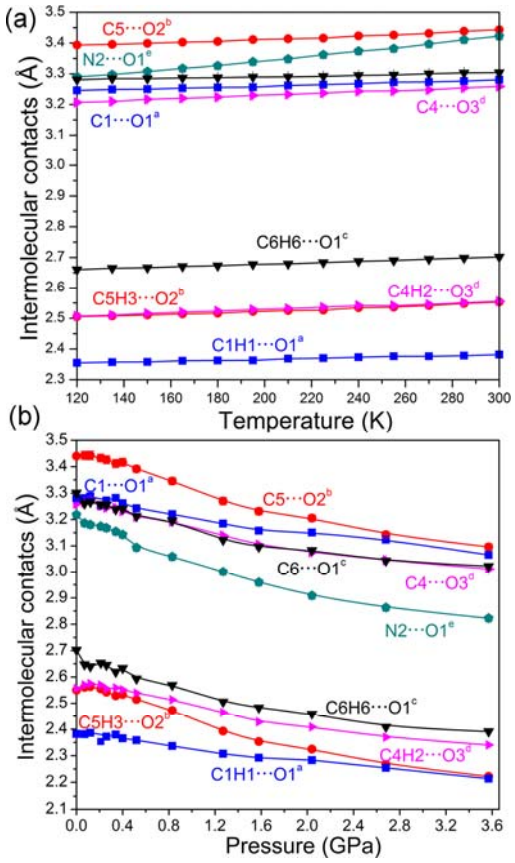

Fig. S9 Distances of intermolecular contacts as a function of (a) temperature and (b) pressure in POM. Symmetey codes: (a) 1/2–*x*, –*y*, *z*–1/2; (b) *x*, *y*–1,1+*z* ; (c) *x*, 1+*y*, *z*–1; (d) –*x*, *y*–1/2, 3/2–*z* and (e) *x*, *y*+1, *z*.

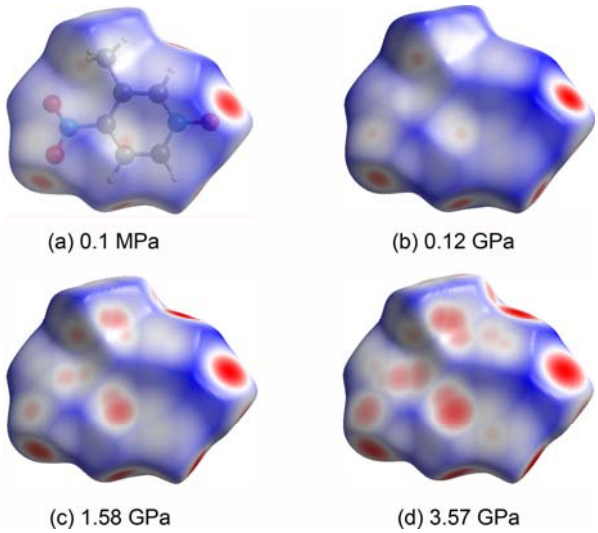

Fig. S10 Normalized intermolecular contacts mapped on the Hirshfeld surfaces of the POM molecule: phase I at (a) 0.1 MPa and (b) 0.12 GPa; as well as in phase II at (c) 1.58 GPa and (d) 3.57 GPa. The colour scale describes distances longer (navy-blue), equal (white), and shorter (red) than the van der Waals radii. The corresponding 2D fingerprint plots are given in Figure S11.

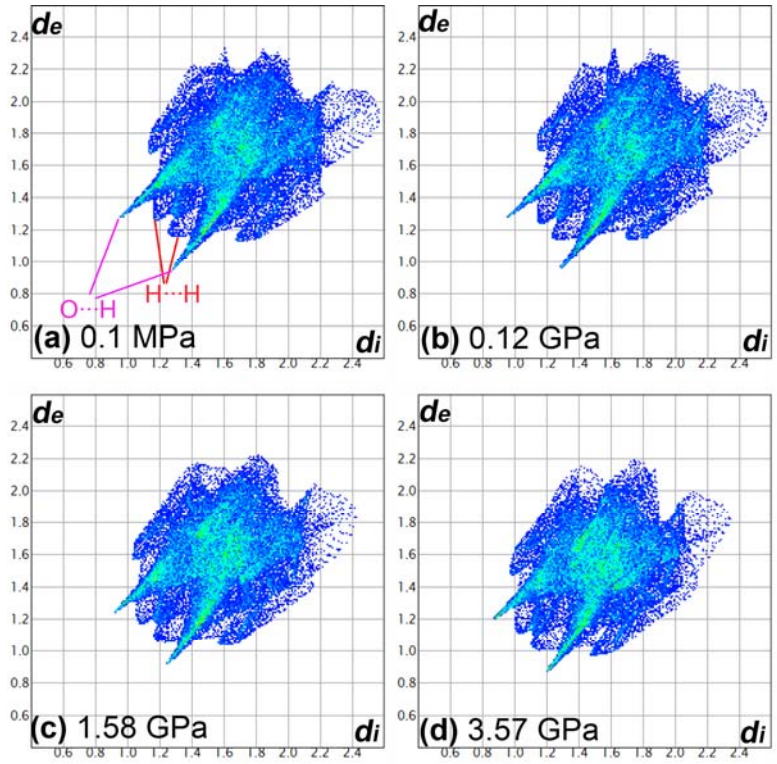

Fig. S11 2D fingerprint plots for the POM crystals in phase I at (a) 0.1 MPa and (b) 0.12 GPa; as well as phase II at (c) 1.58 GPa and (d) 3.57 GPa.

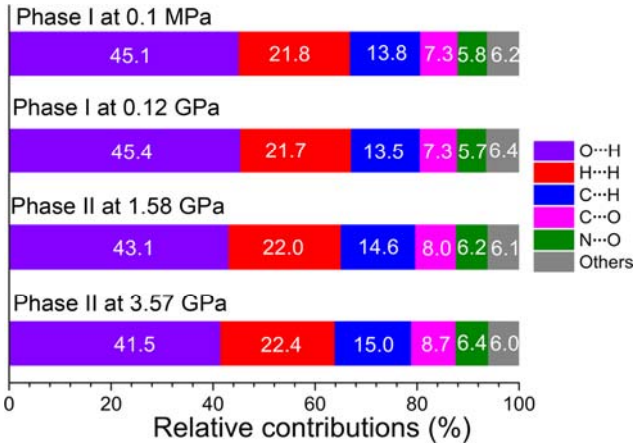

Fig. S12 Relative contributions (%) to the Hirshfeld surface for different types of contacts in phase I at 0.1 MPa and 0.12 GPa; as well as phase II at 1.58 and 3.57 GPa.

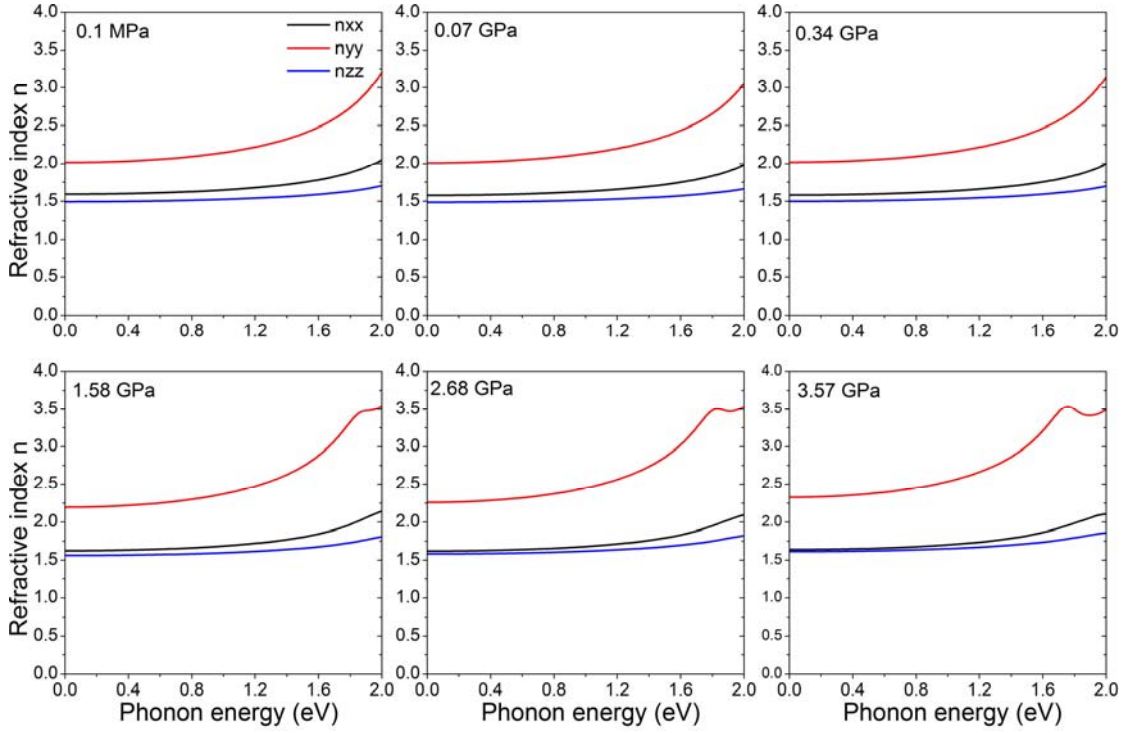

Fig. S13 The calculated refractive index n of the POM crystal at 0.1 MPa, 0.07, 0.34, 1.58, 2.27 and 3.57 GPa.

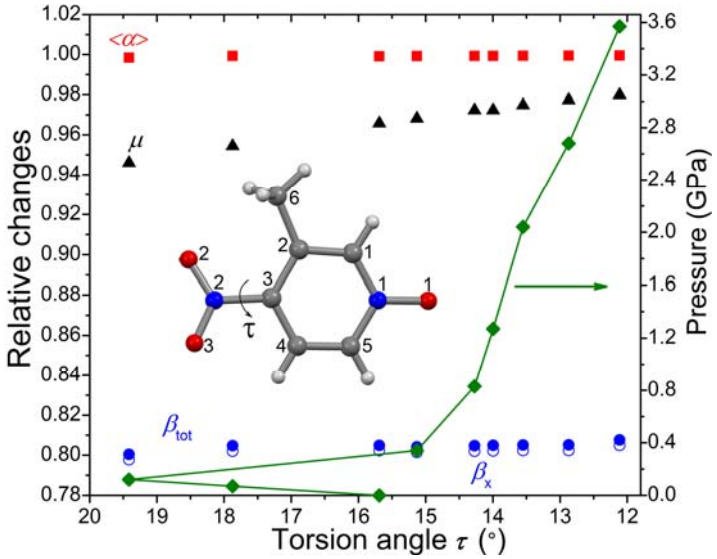

Fig. S14 Changes of molecular second-order polarizability β_{tot} (full circles) and tensor β_x (open circles), dipole moment μ (black triangles), and mean polarizability $<\alpha>$ (full squares) related to the most stable conformer as a function of torsion angle τ(O2−N2−C3−C4) in POM (the left scale). The green diamond symbols indicate the torsion angles as the function of pressure (the right scale). The reference data for the most energetically stable conformer ($\tau = 4.6°$).

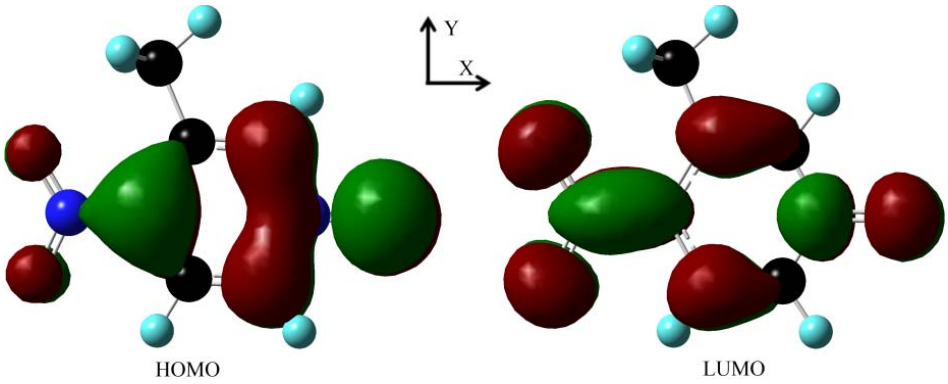

Fig. S15 The main (89%) front orbitals involved in the first dipole-allowed excitation (ΔE^{eg} = 3.8 eV) for the POM most energetically stable conformer (τ = 4.6°).

Table S1. Selected crystallographic data and refinement details of POM between 120 and 300 K.

Temperature (K)	120	135	150	165
Formula	$C_6H_6N_2O_3$			
Crystal system	Orthorhombic			
Space group	$P2_12_12_1$			
a/Å	20.9533(7)	20.9915(8)	21.0223(8)	21.0588(8)
b/Å	6.1092(2)	6.1114(2)	6.1129(2)	6.1144(2)
c/Å	5.1332(2)	5.1337(2)	5.1343(2)	5.1343(2)
V/Å^3	657.09(5)	658.59(4)	659.79(4)	661.10(4)
Z	4			
D_{cal} (g cm^{-3})	1.558	1.554	1.552	1.549
θ range(°)	3.47–28.94	3.47–28.91	3.47–28.89	3.47–28.86
μ (mm^{-1})	0.127	0.127	0.127	0.127
F(000)	320			
R_{int}	0.0122	0.0115	0.0123	0.0122
R_1/wR_2 [I>2σ(I)][a]	0.0282/0.0739	0.0283/0.0752	0.0280/0.0754	0.0281/0.0748
R_1/wR_2 indices (all data)	0.0305/0.0764	0.0298/0.0765	0.0305/0.0768	0.0313/0.0775
Extinction coefficient	0.023(5)	0.025(6)	0.026(6)	0.027(6)
Goodness-of-fit on F_0^2	1.144	1.195	1.127	1.118
Largest peak/hole (e·Å^{-3})	0.19/–0.14	0.20/–0.13	0.22/–0.13	0.18/–0.14
CCDC	979897	979898	979899	979900

Table S1 (continued)

Temperature (K)	180	195	210	225
Formula	$C_6H_6N_2O_3$			
Crystal system	Orthorhombic			
Space group	$P2_12_12_1$			
a/Å	21.0975(9)	21.1324(8)	21.1719(9)	21.2160(9)
b/Å	6.1157(3)	6.1162(2)	6.1190(3)	6.1203(3)
c/Å	5.1353(2)	5.1363(2)	5.1373(3)	5.1381(3)
V/Å^3	662.59(5)	663.87(4)	665.54(6)	667.17(6)
Z	4			
D_{cal} (g cm^{-3})	1.545	1.542	1.538	1.534
θ range(°)	3.47–28.84	3.47–28.81	3.47–28.78	3.46–28.75
μ (mm^{-1})	0.126	0.126	0.126	0.126
F(000)	320			
R_{int}	0.0114	0.0123	0.0119	0.0125
R_1/wR_2 [I>2σ(I)][a]	0.0298/0.0767	0.0302/0.0790	0.0307/0.0811	0.0316/0.0796
R_1/wR_2 indices (all data)	0.0329/0.0794	0.0334/0.0832	0.0347/0.0845	0.0352/0.0828
Extinction coefficient	0.031(6)	0.031(6)	0.029(6)	0.032(6)
Goodness-of-fit on F_0^2	1.118	1.155	1.152	1.173
Largest peak/hole (e·Å^{-3})	0.20/–0.13	0.18/–0.17	0.17/–0.14	0.18/–0.15
CCDC	979901	979902	979903	979904

Table S1 (continued)

Temperature (K)	240	255	270	285	300
Formula	$C_6H_6N_2O_3$				
Crystal system	Orthorhombic				
Space group	$P2_12_12_1$				
a/Å	21.2598(9)	21.2997(10)	21.3430(10)	21.3830(10)	21.4311(11)
b/Å	6.1219(3)	6.1229(3)	6.1262(3)	6.1278(3)	6.1298(3)
c/Å	5.1391(3)	5.1413(3)	5.1430(3)	5.1462(3)	5.1489(3)
V/Å^3	668.86(6)	670.51(6)	672.45(6)	674.31(6)	676.40(6)
Z	4				
D_{cal} (g cm^{-3})	1.531	1.527	1.522	1.518	1.514
θ range(°)	3.46–28.72	3.46–28.70	3.46–28.66	3.46–28.63	3.46–28.60
μ (mm^{-1})	0.125	0.125	0.125	0.124	0.124
F(000)	320				
R_{int}	0.0143	0.0116	0.0131	0.0121	0.0129
R_1/wR_2 [I>2σ(I)][a]	0.0311/0.0804	0.0319/0.0845	0.0314/0.0813	0.0338/0.0875	0.0338/0.0847
R_1/wR_2 indices (all data)	0.0364/0.0859	0.0371/0.0876	0.0374/0.0863	0.0397/0.0919	0.0409/0.0895
Extinction coefficient	0.034(6)	0.032(7)	0.035(6)	0.033(7)s	0.034(6)
Goodness-of-fit on F_0^2	1.130	1.101	1.119	1.087	1.103
Largest peak/hole (e·Å^{-3})	0.16/–0.12	0.15/–0.14	0.14/–0.13	0.14/–0.12	0.15/–0.12
CCDC	979905	979906	979907	979868	979869

[a] $R_1=\sum||F_o|-|F_c||/\sum|F_o|$ for $F_o^2>2\sigma(F_o^2)$; $wR_2=\sum[w(F_o^2-F_c^2)]/\sum[w(F_o^2)^2]^{1/2}$,where $w= 1/[\sigma^2F_o^2+(A\ P)^2+ BP]$, and $P = (Fo^2+ 2Fc^2)/3$

Table S2. Selected crystallographic data and refinement details of POM at variable pressure, all at 296 K.

Pressure (GPa)	0.0001	0.07	0.12	0.21	0.26
Formula	$C_6H_6N_2O_3$				
Crystal system	Orthorhombic				
Space group	$P2_12_12_1$				
a/Å	21.4235(4)	21.363(5)	21.325(5)	21.267(5)	21.215(4)
b/Å	6.1275(1)	6.141(5)	6.152(6)	6.133(5)	6.128(5)
c/Å	5.1487(1)	5.1404(11)	5.1306(10)	5.1284(12)	5.1180(11)
V/Å^3	675.88(2)	674.4(6)	673.1(7)	668.9(6)	665.4(6)
Z	4				
D_{cal} (g cm^{-3})	1.515	1.518	1.521	1.531	1.539
θ range(º)	1.90–26.49	3.82–27.45	3.82–27.98	5.52–27.09	3.84–27.16
μ (mm^{-1})	0.124	0.124	0.124	0.125	0.126
F(000)	320				
R_{int}	0.0209	0.0662	0.0746	0.1065	0.0711
R_1/wR_2 [I>2σ(I)][a]	0.0343/0.0804	0.0571/0.1136	0.0621/0.0780	0.0499/0.1061	0.0457/0.0969
R_1/wR_2 indices(all data)	0.0411/0.0825	0.0778/0.1280	0.0862/0.0846	0.0591/0.1137	0.0626/0.1076
Extinction coefficient	0.035(6)	–	0.078(8)	–	0.067(15)
Goodness-of-fit on F_0^2	1.244	1.171	1.308	1.164	1.151
Largest peak/hole (e·Å^{-3})	0.14/–0.13	0.10/–0.11	0.06/–0.06	0.11/–0.11	0.07/–0.08
CCDC	979870	979871	979872	979873	979874

Table S2 (continued)

Pressure (GPa)	0.34	0.40	0.52	0.83	1.29
Formula	$C_6H_6N_2O_3$				
Crystal system	Orthorhombic				
Space group	$P2_12_12_1$				
a/Å	21.148(5)	21.101(4)	20.994(8)	20.771(4)	20.5114(19)
b/Å	6.121(5)	6.112(5)	6.105(7)	6.075(4)	6.016(4)
c/Å	5.1082(12)	5.0990(9)	5.0903(18)	5.0621(10)	5.005(2)
V/Å^3	661.3(6)	657.7(6)	652.5(8)	638.7(4)	617.6(5)
Z	4				
D_{cal} (g cm^{-3})	1.548	1.557	1.569	1.603	1.658
θ range(º)	3.85–27.16	3.86–27.22	3.88–27.14	4.99–27.04	3.97–28.24
μ (mm^{-1})	0.127	0.127	0.128	0.131	0.136
F(000)	320				
R_{int}	0.0715	0.0734	0.1983	0.0956	0.0940
R_1/wR_2 [I>2σ(I)][a]	0.0512/0.1003	0.0554/0.0943	0.0555/0.1165	0.0621/0.0912	0.0405/0.0662
R_1/wR_2 indices(all data)	0.0697/0.1104	0.0674/0.0994	0.0777/0.1276	0.0751/0.0950	0.0564/0.0709
Extinction coefficient	0.072(14)	0.094(12)	–	–	–
Goodness-of-fit on F_0^2	1.203	1.071	1.095	1.220	1.173
Largest peak/hole (e·Å^{-3})	0.08/–0.06	0.08/–0.07	0.08/–0.09	0.07/–0.07	0.05/–0.06
CCDC	979875	979876	979877	979878	979908

Table S2 (continued)

Pressure (GPa)	1.58	2.04	2.68	3.57
Crystal system	Orthorhombic			
Formula	$C_6H_6N_2O_3$			
Space group	$P2_12_12_1$			
a/Å	20.343(2)	20.141(2)	19.878(3)	19.5490(16)
b/Å	6.001(4)	5.973(5)	5.938(4)	5.901(4)
c/Å	4.9855(17)	4.9650(18)	4.9394(14)	4.9131(14)
V/Å^3	608.6(5)	597.3(5)	583.0(4)	566.7(4)
Z	4			
D_{cal} (g cm^{-3})	1.682	1.714	1.756	1.806
θ range(°)	4.21–27.18	4.23–27.37	4.25–27.61	4.28–27.19
μ (mm^{-1})	0.138	0.140	0.144	0.148
F(000)	320			
R_{int}	0.0810	0.0799	0.0715	0.0635
R_1/wR_2 [I>2σ(I)][a]	0.0312/0.0560	0.0343/0.0700	0.0363/0.0758	0.0388/0.0776
R_1/wR_2 indices(all data)	0.0397/0.0598	0.0422/0.0757	0.0428/0.0793	0.0451/0.0809
Extinction coefficient	–	–	–	–
Goodness-of-fit on F_0^2	1.072	1.069	1.143	1.205
Largest peak/hole (e·Å^{-3})	0.07/–0.07	0.07/–0.08	0.09/–0.10	0.11/–0.09
CCDC	979909	979910	979911	979912

[a] $R_1=\sum||F_o|-|F_c||/\sum|F_o|$ for $F_o^2>2\sigma(F_o^2)$; $wR_2=\sum[w(F_o^2-F_c^2)]/\sum[w(F_o^2)^2]^{1/2}$,where $w= 1/[\sigma^2F_o^2+(AP)^2+BP]$, and $P = (Fo^2+2Fc^2)/3$

Table S3. Reported intrinsic NLC in organic crystals and other materials.

Compound	axis	β (TPa^{-1})	Pressure range (GPa)	Reference
Organic materials				
POM	*b*	−33(2)	0−0.12	This work
Methanol monohydrate	*a*	−3.8(5)	0−0.5	21
Methyl benzoate	*b*	−16.5(3)	0.38−0.52	22
2-(3'-chlorophenyl) imidazoline	*a*	−14.3	0−0.08	23
	b	−5.2		
1,3-Cyclohexanedione	*c*	−29(2)	0.11−0.52	24
Acetaminophen	~*c*	−17(3)	2.0−4.0	25
Inorganic materials				
$KMn[Ag(CN)_2]_3$	*c*	−12.0(8)	0−2.2	26
$Ag_3[Co(CN)_6]$-I	~*c*	−76(9)	0−0.19	27
$Ag_3[Co(CN)_6]$-II	~*c*	−5.3(3)	0.19−7.6	
$Zn[Au(CN)_2]_2$-I	*c*	−42(5)	0−1.8	28
$Zn[Au(CN)_2]_2$-II	*c*	−6(3)	1.8−14.2	
MOFs				
Silver(I) 2-methylimidazolate	~*c*	−4.32(10)	0−1.0	29
$[NH_4][Zn(HCOO)_3]$	*c*	−1.8(8)	0−0.94	30
$Zn(HO_3PC_4H_8PO_3H)\cdot 2H_2O$	*b*	−15.8	1.65−2.81	31
Metal complexes				
$[Fe(dpp)_2(NCS)_2]\cdot$py*	~*a*	−10.3	0−2.48	32
$[(C_6F_5Au)_2(DCB)]$**	*a*	−12.57	0−2.42	33
		−4.16	0−4.39	

*dpp = dipyrido[3,2-a:2'3'-c]phenazine and py = pyridine); **DCB = μ-1,4-diisocyanobenzene.

Table S4. The torsion angles τ (º) of POM at variable temperature and pressure.

Temperature (K)	Torsion angle (º)	Pressure (GPa)	Torsion angle (º)
120	14.75(17)	0.0001	15.7(1)
135	14.76(17)	0.07	17.9(8)
150	14.77(18)	0.12	19.4(8)
165	14.86(18)	0.21	16.3(7)
180	14.88(19)	0.26	15.5(7)
195	14.97(20)	0.34	15.1(7)
210	14.99(20)	0.40	15.2(8)
225	15.13(21)	0.52	15.1(7)
240	15.21(21)	0.83	14.3(8)
255	15.17(22)	1.29	14.0(6)
270	15.34(22)	1.58	13.8(6)
285	15.45(23)	2.04	13.6(5)
300	15.48(24)	2.68	12.9(5)
		3.57	12.1(5)

Table S5. Intermolecular contacts as a function of temperature

T (K)	120	135	150	165	180	195	210
C1–H1···O1[a]							
D–H	0.93	0.93	0.93	0.93	0.93	0.93	0.93
H···A	2.355	2.357	2.358	2.361	2.363	2.363	2.369
D···A	3.246(2)	3.249(2)	3.250(2)	3.254(2)	3.256(2)	3.257(2)	3.263(2)
D–H···A	160.4	160.7	160.8	160.7	161.0	161.0	161.1
C5–H3···O2[b]							
D–H	0.93	0.93	0.93	0.93	0.93	0.93	0.93
H···A	2.505	2.508	2.511	2.514	2.517	2.522	2.525
D···A	3.394(2)	3.396(2)	3.399(2)	3.403(2)	3.405(2)	3.411(2)	3.414(2)
D–H···A	159.9	159.8	159.9	159.9	159.9	160.1	160.0
C6–H6···O1[c]							
D–H	0.93	0.93	0.93	0.93	0.93	0.93	0.93
H···A	2.660	2.665	2.666	2.671	2.673	2.677	2.679
D···A	3.281(2)	3.285(2)	3.285(2)	3.286(2)	3.288(2)	3.290(2)	3.290(2)
D–H···A	122.8	122.7	122.6	122.4	122.3	122.1	122.0
C4–H2···O3[d]							
D–H	0.93	0.93	0.93	0.93	0.93	0.93	0.93
H···A	2.507	2.510	2.516	2.520	2.524	2.529	2.532
D···A	3.207(2)	3.210 (2)	3.217(2)	3.221(2)	3.225(2)	3.230(2)	3.234(2)
D–H···A	132.3	132.3	132.4	132.3	132.4	132.5	132.5
N2···O1[e]	3.290(2)	3.297(2)	3.307(2)	3.317(2)	3.326(2)	3.339(2)	3.348(2)

Table S5 (continued)

T (K)	225	240	255	270	285	300
C1–H1···O1[a]						
D–H	0.93	0.93	0.93	0.93	0.93	0.93
H···A	2.369	2.373	2.376	2.376	2.378	2.382
D···A	3.264(2)	3.268(2)	3.273(2)	3.274(2)	3.277(2)	3.280(2)
D–H···A	161.37	161.4	161.8	162.0	162.3	162.5
C5–H3···O2[b]						
D–H	0.93	0.93	0.93	0.93	0.93	0.93
H···A		2.535	2.536	2.542	2.548	2.553
D···A	3.414(2)	3.424(2)	3.426(2)	3.432(2)	3.439(2)	3.443(2)
D–H···A	160.0	160.0	160.3	160.3	160.4	160.4
C6–H6···O1[c]						
D–H	0.93	0.93	0.93	0.93	0.93	0.93
H···A	2.683	2.688	2.690	2.695	2.698	2.702
D···A	3.292(2)	3.295(2)	3.2963(2)	3.3004(2)	3.3031(2)	3.3041(2)
D–H···A	121.6	121.7	121.6	121.6	121.5	121.3
C4–H2···O3[d]						
D–H	0.93	0.93	0.93	0.93	0.93	0.93
H···A	2.536	2.542	2.542	2.545	2.551	2.555
D···A	3.237(2)	3.244(2)	3.245(2)	3.248(2)	3.255(2)	3.259(2)
D–H···A	132.3	132.5	132.7	132.7	132.8	132.7
N2···O1[e]	3.362(2)	3.374(2)	3.382(2)	3.397(2)	3.411(2)	3.422(2)

Symmetey codes: (a) 1/2–*x*, –*y*, –1/2+*z*; (b) *x*, –1+*y*,1+*z* ; (c) *x*, 1+*y*, –1+*z* ; (d) –*x*, –1/2+*y*, 3/2–*z* and (e) *x*, *y*+1, *z*.

Table S6. Intermolecular contacts as a function of pressure

P (GPa)	0.0001	0.07	0.12	0.21	0.26	0.34
C1–H1···O1[a]						
D–H	0.93	0.93	0.93	0.93	0.93	0.93
H···A	2.382	2.381	2.386	2.353	2.371	2.379
D···A	3.280(2)	3.281(7)	3.287(7)	3.254(8)	3.271(6)	3.281(7)
D–H···A	162.3	162.7	163.2	163.0	163.2	163.3
C5–H3···O2[b]						
D–H	0.93	0.93	0.93	0.93	0.93	0.93
H···A	2.550	2.561	2.564	2.555	2.542	2.529
D···A	3.440(2)	3.443(16)	3.443(16)	3.433(15)	3.426(15)	3.412(15)
D–H···A	160.4	158.3	157.8	157.5	158.9	158.7
C6–H6···O1[c]						
D–H	0.93	0.93	0.93	0.93	0.93	0.93
H···A	2.702	2.647	2.640	2.653	2.645	2.619
D···A	3.301(2)	3.260(15)	3.266(16)	3.257(14)	3.255(14)	3.238(13)
D–H···A	121.0	122.0	123.2	121.3	121.8	122.5
C4–H2···O3[d]						
D–H	0.93	0.93	0.93	0.93	0.93	0.93
H···A	2.556	2.570	2.575	2.570	2.555	2.559
D···A	3.260(2)	3.264(8)	3.278(7)	3.252(6)	3.245(6)	3.243(7)
D–H···A	132.7	131.8	132.8	131.1	131.3	130.7
N2···O1[e]	3.218(2)	3.186(9)	3.180(90	3.174(9)	3.168(9)	3.155(8)

Table S6 (continued)

P (GPa)	0.40	0.52	0.83	1.29	1.58	2.04	2.68	3.57
C1–H1···O1[a]								
D–H	0.93	0.93	0.93	0.93	0.93	0.93	0.93	0.93
H···A	2.365	2.358	2.337	2.307	2.292	2.283	2.254	2.213
D···A	3.261(7)	3.242(6)	3.220(8)	3.184(4)	3.158(5)	3.150(5)	3.124(5)	3.065(5)
D–H···A	161.7	157.8	158.5	157.1	154.6	154.9	155.4	151.9
C5–H3···O2[b]								
D–H	0.93	0.93	0.93	0.93	0.93	0.93	0.93	0.93
H···A	2.533	2.515	2.473	2.393	2.354	2.325	2.267	2.222
D···A	3.417(15)	3.391(13)	3.346(13)	3.270(13)	3.231(13)	3.205(12)	3.143(12)	3.096(12)
D–H···A	158.5	157.3	156.3	157.1	157.2	157.8	156.6	156.28
C6–H6···O1[c]								
D–H	0.93	0.93	0.93	0.93	0.93	0.93	0.93	0.93
H···A	2.634	2.593	2.569	2.506	2.483	2.459	2.408	2.391
D···A	3.240(14)	3.212(15)	3.195(14)	3.122(15)	3.096(13)	3.083(13)	3.043(13)	3.022(14)
D–H···A	121.5	122.5	123.0	121.9	121.6	122.5	123.3	122.9
C4–H2···O3[d]								
D–H	0.93	0.93	0.93	0.93	0.93	0.93	0.93	0.93
H···A	2.552	2.539	2.514	2.465	2.428	2.408	2.369	2.340
D···A	3.233(8)	3.210(7)	3.193(8)	3.139(6)	3.104(5)	3.076(5)	3.046(5)	3.011(5)
D–H···A	129.9	129.3	130.0	129.4	129.6	128.6	129.3	128.7
N2···O1[e]	3.143(9)	3.093(9)	3.059(9)	3.000(9)	2.959(9)	2.909(8)	2.863(8)	2.823(8)

Symmetey codes: (a) 1/2–*x*, –*y*, –1/2+*z*; (b) *x*, –1+*y*,1+*z*; (c) *x*, 1+*y*, –1+*z*; (d) –*x*, –1/2+*y*, 3/2–*z* and (e) *x*, *y*+1, *z*.

Table S7. The calculated molecular energy and static dipolar polarizability components, mean polarizability $\langle\alpha\rangle$ and anisotropy of polarizability $\Delta\alpha$ (a.u.) of POM from selected high-pressure data.

P (GPa)	Energy (a.u.)	μ_x	μ_y	μ_z	μ	α_{xx}	α_{yy}	α_{zz}	$\langle\alpha\rangle$
0.0001	–567.4263658	0.2596	0.3748	0.0223	0.4565	158.93	109.64	53.15	107.24
0.07	–567.4263332	0.2521	0.3732	0.0252	0.4511	159.05	109.75	52.99	107.26
0.12	–567.4263018	0.2462	0.3722	0.0273	0.4471	158.60	109.27	53.64	107.17
0.34	–567.4263723	0.2612	0.3751	0.0216	0.4576	158.98	109.68	53.09	107.25
0.83	–567.4263809	0.2639	0.3757	0.0202	0.4596	159.05	109.75	52.99	107.26
1.29	–567.4263833	0.2641	0.3756	0.0197	0.4596	159.06	109.77	52.95	107.26
2.04	–567.4263869	0.2658	0.3759	0.0183	0.4607	159.09	109.81	52.91	107.27
2.68	–567.4263918	0.2674	0.3763	0.0170	0.4619	159.14	109.86	52.83	107.28
3.57	–567.4263964	0.2690	0.3766	0.0171	0.4632	159.18	109.92	52.76	107.28
gas phase	–567.4264114	0.2821	0.3792	0.0059	0.4726	159.49	110.29	52.22	107.33

Table S8. Static first-order hyperpolarizability components, total second-order polarizability β_{tot} (a.u.) of POM from selected high-pressure data.

P (GPa)	β_{xxx}	β_{xxy}	β_{xyy}	β_{yyy}	β_{xxz}	β_{xyz}	β_{yyz}	β_{xzz}	β_{yzz}	β_{zzz}
0.0001	–1297.76	–123.87	148.23	–31.81	0.22	3.11	–4.36	–13.01	–6.24	–2.47
0.07	–1298.93	–124.35	149.50	–32.13	–0.16	2.90	–4.00	–12.79	–6.36	–2.38
0.12	–1290.06	–123.99	145.82	–31.08	–0.38	3.56	–4.93	–11.86	–6.04	–2.92
0.34	–1297.64	–124.30	148.95	–31.97	–0.21	3.04	–4.17	–12.65	–6.31	–2.46
0.83	–1298.93	–124.35	149.50	–32.13	–0.16	2.90	–4.00	–12.79	–6.36	–2.38
1.29	–1299.28	–124.35	149.67	–32.16	–0.11	2.86	–3.92	–12.84	–6.38	–2.35
2.04	–1299.75	–124.38	149.97	–32.26	–0.08	2.79	–3.82	–12.91	–6.40	–2.33
2.68	–1300.34	–124.58	150.50	–32.31	–0.16	2.61	–3.65	–12.88	–6.44	–2.25
3.57	–1303.16	–124.02	150.38	–32.42	0.38	2.53	–3.59	–13.64	–6.44	–2.02
gas phase	–1309.13	–123.90	–153.82	–33.35	0.51	–0.95	–1.47	13.90	–6.73	–0.88

Table S8 (continued)

P (GPa)	β_x	β_y	β_z	β_{tot}
0.0001	–1162.55	–161.92	–6.61	1173.79
0.07	–1162.22	–162.84	–6.54	1173.59
0.12	–1156.09	–161.11	–8.23	1167.29
0.34	–1161.34	–162.58	–6.84	1172.69
0.83	–1162.22	–162.84	–6.54	1173.59
1.29	–1162.45	–162.88	–6.38	1173.82
2.04	–1162.69	–163.04	–6.23	1174.08
2.68	–1162.72	–163.32	–6.07	1174.15
3.57	–1166.42	–162.88	–5.23	1177.75
gas phase	–1449.04	–163.98	–1.84	1458.29

Table S9. Changes of dipole moment from the ground state to excited state ($\Delta\mu_x^{eg}$), transition energy (ΔE^{eg}), oscillator strength (*f*), transition dipole moment (M_{xx}^{eg}) and the contribution (C_i) of HOMO and LUMO to the lowest dipole-allowed excited state for three conformers with selected torsion angles τ fixed at 4.6°, 12.1° and 19.4° (cf. Table S4).

Pressure	τ (°)	$\Delta\mu_x^{eg}$ (D)	ΔE^{eg} (eV)	f	M_{xx}^{eg} (D)	C_i
gas phase	4.6	3.5957	3.8028	0.2935	3.1502	89.2%
3.57 GPa	12.1	2.4244	3.8352	0.2199	2.3401	65.4%
0.12 GPa	19.4	1.4434	3.8794	0.1614	1.6976	45.8%

References

1 L. Merrill and W. A. Bassett., *Rev. Sci. Instrum.*, 1974, **45**, 290.
2 L. W. Finger and R. M. Hazen, *J. Appl. Phys.*, 1978, **49**, 5823.
3 G. J. Piermarini, S. Block, J. D. Barnett and R. A. Forman, *J. Appl. Phys.* 1975, **46**, 2774.
4 D. Zhang, G. Lan, S. Hu, H. Wang and J. Zheng, *J. Raman Spectrosc.* 1994, **25**, 327.
5 D. R. Allan, S. J. Clark, M. J. P. Brugmans, G. J. Ackland and W. L. Vos, *Phys. Rev. B*, 1998, **58**, 11809.
6 A. Budzianowski and A. Katrusiak, *High-Pressure Crystallography*, eds. A. Katrusiak and P. F. McMillan, Kluwer Academic Publishers, Dordrecht, 2004, pp. 101–112.
7 Oxford Diffraction, *Version 1.171*, Oxford Diffraction Ltd: Abingdon, Oxfordshire, UK, 2004.
8 (a) A. Katrusiak, *Z. Kristallogr.* 2004, **219**, 461; (b) A. Katrusiak, *A program for correcting reflections intensities for DAC absorption and gasket shadowing*, Adam Mickiewicz University, Poznań, Poland, 2003.
9 J. C. Tan, C. A. Merrill, J. B. Orton and A. K. Cheetham, *Acta Mater.* 2009, **57**, 3481.
10 T. Juliano, Y. Gogotsi and V. Dominich, *J. Mater. Res.* 2003, **18**, 1192.
11 J. Klimeš, D. R. Bowler and A. Michaelides, *Phys. Rev. B*, 2011, **83**, 195131.
12 G. Kresse and D. Joubert, *Phys. Rev. B*, 1999, **59**, 1758.
13 P. E. Blöchl, *Phys. Rev. B*, 1994, **50**, 17953.
14 J. P. Perdew, K. Burke and M. Ernzerhof, *Phys. Rev. Lett.*, 1996, **77**, 3865.
15 R. Y. Boyd, Principles of Nonlinear Optics, Academic Press, NY, 1982, p. 420.
16 R. W. Boyd, Nonlinear Optics; Academic Press: New York, 1992; pp 21–47.
17 M. A. Robb, J. R. Cheeseman, J. A. Montgomery, T. V. Jr., K. N. Kudin, J. C. Burant, J. M. Millam, S. S. Iyengar, J. Tomasi, V. Barone, B. Mennucci, M. Cossi, G. Scalmani, N. Rega, G. A. Petersson, H. Nakatsuji, M. Hada, M. Ehara, K. Toyota, R. Fukuda, J.

Hasegawa, M. Ishida, T. Nakajima, Y. Honda, O. Kitao, H. Nakai, M. Klene, X. Li, J. E. Knox, H. P. Hratchian, J. B. Cross, V. Bakken, C. Adamo, J. Jaramillo, R. Gomperts, R. E. Stratmann, O. Yazyev, A. J. Austin, R. Cammi, C. Pomelli, J. W. Ochterski, P. Y. Ayala, K. Morokuma, G. A. Voth, P. Salvador, J. J. Dannenberg, V. G. Zakrzewski, S. Dapprich, A. D. Daniels, M. C. Strain, O. Farkas, D. K. Malick, A. D. Rabuck, K. Raghavachari, J. B. Foresman, J. V. Ortiz, Q. Cui, A. G. Baboul, S. Clifford, J. Cioslowski, B. B. Stefanov, G. Liu, A. Liashenko, P. Piskorz, I. Komaromi, R. L. Martin, D. J. Fox, T. Keith, M. A. Al-Laham, C. Y. Peng, A. Nanayakkara, M. Challacombe, P. M. W. Gill, B. Johnson, W. Chen, M. W. Wong, C. Gonzalez and J. A. Pople, Gaussian 03, Revision D.01, Gaussian, Inc., Wallingford CT, 2004.

18 (a) G. Berthier, M. Defranceschi, P. Lazzeretti, G. Tsoucaris and R. Zanasi, *J. Mol. Struct.(THEOCHEM)*. 1992, **254,** 205; (b) B. Champagne, E. A. Perpete, T. Legrand, D. Jacquemin, J.-M. Andre, *J. Chem. Soc., Faraday Trans.* 1998, **94**, 1547.

19 J. B. Foresman, M. Head-Gordon, J. A. Pople, M. J. Frisch, *J. Phys. Chem.* 1992, **96**, 135.

20 M. J. Cliffe and A. L. Goodwin, *J. Appl. Cryst.* 2012, **45**, 1321.

21 A. D. Fortes, E. Suard and K. S. Knight, *Science*, 2011, **331**, 742.

22 W. Cai and A. Katrusiak, *J. Phys. Chem. C.*, 2013, **117**, 21460.

23 M. Anioła, A. Katrusiak and R. Kia, *CrystEngComm*, 2012, **14**, 6424.

24 A. Katrusiak, *Acta Crystallogr., Sect. B: Struct. Sci.*, 1990, **46**, 246.

25 E. V. Boldyreva, T. P. Shakhtshneider, M. A. Vasilchenko, H. Ahsbahs and H. Uchtmann, *Acta Crystallogr., Sect. B: Struct. Sci.*, 2000, **56**, 299.

26 A. B. Cairns, A. L. Thompson, M. G. Tucker, J. Haines and A. L. Goodwin, *J. Am. Chem. Soc.*, 2011, **134**, 4454.

27 A. L. Goodwin, D. A. Keen and M. G. Tucker, *Proc. Natl. Acad. Sci.USA*, 2008, **105**, 18708.

28 A. B. Cairns, J. Catafesta, C. Levelut, J. Rouquette, A. van der Lee, L. Peters, A. L. Thompson, V. Dmitriev, J. Haines and A. L. Goodwin, *Nat Mater.*, 2013, **12**, 212.

29 J. M. Ogborn, I. E. Collings, S. A. Moggach, A. L. Thompson and A. L. Goodwin, *Chem. Sci.*, 2012, **3**, 3011.

30 W. Li, M. R. Probert, M. Kosa, T. D. Bennett, A. Thirumurugan, R. P. Burwood, M. Parinello, J. A. K. Howard and A. K. Cheetham, *J. Am. Chem. Soc.*, 2012, **134**, 11940.

31 K. J. Gagnon, C. M. Beavers and A. Clearfield, *J. Am. Chem. Soc.*, 2013, **135**, 1252.

32 H. J. Shepherd, T. Palamarciuc, P. Rosa, P. Guionneau, G. Molnár, J.-F. Létard and A. Bousseksou, *Angew. Chem. Int. Ed.*, 2012, **51**, 3910.

33 C. H. Woodall, C. M. Beavers, J. Christensen, L. E. Hatcher, M. Intissar, A. Parlett, S. J. Teat, C. Reber and P. R. Raithby, *Angew. Chem. Int. Ed.*, 2013, **52**, 1.